On Probing Signal Design For MIMO Radar

Petre Stoica, *Fellow, IEEE*, Jian Li, *Fellow, IEEE*, and Yao Xie, *Student Member, IEEE*

***Abstract*—A multiple-input multiple-output (MIMO) radar system, unlike a standard phased-array radar, can choose freely the probing signals transmitted via its antennas to maximize the power around the locations of the targets of interest, or more generally to approximate a given transmit beampattern, and also to minimize the cross-correlation of the signals reflected back to the radar by the targets of interest. In this paper, we show how the above desirable features can be achieved by designing the covariance matrix of the probing signal vector transmitted by the radar. Moreover, in a numerical study, we show that the proper choice of the probing signals can significantly improve the performance of adaptive MIMO radar techniques. Additionally, we demonstrate the advantages of several MIMO transmit beampattern designs, including a beampattern matching design and a minimum sidelobe beampattern design, over their phased-array counterparts.**

***Index Terms*—Beampattern matching design, multiple-input multiple-output (MIMO) radar, minimum sidelobe beampattern design, probing signal design, transmit beampattern.**

I. Introduction

THE multiple-input multiple-output (MIMO) radar is an emerging technology that is attracting the attention of researchers and practitioners alike due to its improved capabilities compared with a standard phased-array radar; see, e.g., [1]–[7]. In particular, as shown recently in [6], a MIMO radar makes it possible to use *adaptive* localization and detection techniques, unlike a phased-array radar. In addition, the probing signal vector transmitted by a MIMO radar system can be designed to approximate a desired transmit beampattern and also to minimize the cross-correlation of the signals bounced from various targets of interest—an operation that, once again, would be hardly possible for a phased-array radar.

The probing signal design problem for the narrow-band MIMO radar has been addressed in, e.g., [3] and [5]. It is also the main topic of this paper. Our approach to this design problem is similar to the mathematical approach of [3] and is different from the more pragmatical approach of [5]. Compared with [3], our main contributions are the following: 1) we address the question of determining a desirable transmit beampattern, and show how to obtain such a beampattern; 2) we modify the beampattern matching criterion of [3] in several ways; in particular, we include a new term in the said criterion that involves the cross-correlation between the signals bounced back to the radar from the targets of interest; and 3) we outline an efficient Semi-Definite Quadratic Programming (SQP) algorithm for solving the signal design problem in polynomial time (the recent full version [8] of [3] also considers a convex optimization algorithm for solving the design problem, yet one that is less efficient than the SQP algorithm proposed herein). In addition, we consider a minimum sidelobe beampattern design, which is not considered in [3] or [8]. Finally, we demonstrate the advantages of these MIMO transmit beampattern designs over their phased-array counterparts. In the sections to follow, we will discuss these contributions in detail.

Manuscript received April 28, 2006; revised October 25, 2006. This work was supported in part by the National Science Foundation under Grant CCF-0634786. The associate editor coordinating the review of this manuscript and approving it for publication was Dr. Daniel Fuhrman.

P. Stoica is with the Department of Information Technology, Uppsala University, SE-751 05 Uppsala, Sweden (e-mail: peter.stoica@it.uu.se).

J. Li is with the Department of Electrical and Computer Engineering, University of Florida, Gainesville, FL 32611-6130 USA (e-mail: li@dsp.ufl.edu).

Y. Xie was with the Department of Electrical and Computer Engineering, University of Florida, Gainesville, FL 32611-6130 USA. She is now with the Department of Electrical Engineering, Stanford University, Stanford, CA 94305 USA (e-mail: yaoxie@stanford.edu).

Color versions of one or more of the figures in this paper are available online at http://ieeexplore.ieee.org.

Digital Object Identifier 10.1109/TSP.2007.894398

II. Problem Formulation

Consider a MIMO radar system with M transmit antennas and let $x_m(n)$ denote the discrete-time base-band signal transmitted by the mth antenna. Also, let θ denote the location parameter(s) of a generic target, for example, its azimuth angle and its range. Then, under the assumption that the transmitted probing signals are narrow-band and that the propagation is nondispersive, the base-band signal at the target location can be described by the expression (see, e.g., [9, Ch. 6])

$$\sum_{m=1}^{M} e^{-j2\pi f_0 \tau_m(\theta)} x_m(n) \triangleq \mathbf{a}^*(\theta)\mathbf{x}(n), \quad n = 1, \ldots, N \tag{1}$$

where f_0 is the carrier frequency of the radar, $\tau_m(\theta)$ is the time needed by the signal emitted via the mth transmit antenna to arrive at the target, $(\cdot)^*$ denotes the conjugate transpose, N denotes the number of samples of each transmitted signal pulse

$$\mathbf{x}(n) = [\, x_1(n) \quad x_2(n) \quad \ldots \quad x_M(n) \,]^T \tag{2}$$

and

$$\mathbf{a}(\theta) = [\, e^{j2\pi f_0 \tau_1(\theta)} \quad e^{j2\pi f_0 \tau_2(\theta)} \quad \ldots \quad e^{j2\pi f_0 \tau_M(\theta)} \,]^T \tag{3}$$

with $(\cdot)^T$ denoting the transpose. Assuming that the transmit array of the radar is calibrated, $\mathbf{a}(\theta)$ is a known function of θ.

It follows from (1) that the power of the probing signal at a generic focal point with location θ is given by

Spatial spectrum

$$P(\theta) = \mathbf{a}^*(\theta)\mathbf{R}\mathbf{a}(\theta), \tag{4}$$

where $\mathbf{R}$ is the covariance matrix of $\mathbf{x}(n)$, i.e.,

$$\mathbf{R} = E\{\mathbf{x}(n)\mathbf{x}^*(n)\}. \tag{5}$$

1053-587X/$25.00 © 2007 IEEE

The "spatial spectrum" in (4), as a function of θ, will be called the *transmit beampattern* (a more detailed derivation of, and further discussions on, (1)–(5) above can be found in [3], [8]).

One of our problems consists of choosing $\mathbf{R}$, under a uniform elemental power constraint

$$R_{mm} = \frac{c}{M}, \quad m = 1, \ldots, M; \text{ with } c \text{ given} \tag{6}$$

where R_{mm} denotes the (m,m)th element of $\mathbf{R}$, to achieve the following goals.

(a) Maximize the total spatial power at a number of given target locations, or more generally, match a desired transmit beampattern.

(b) Minimize the cross-correlation between the probing signals at a number of given target locations; note from (1) that the covariance between the probing signals at locations θ and $\bar{\theta}$ is given by $\mathbf{a}^*(\theta)\mathbf{R}\mathbf{a}(\bar{\theta})$.

According to (a) above, we would like to choose $\mathbf{R}$ such that the available transmit power is used to maximize the probing signal power at the locations of the targets of interest and to minimize it anywhere else. This is a natural goal that needs no additional comments. Regarding (b), we note from [6] and its references that the statistical performance of any adaptive MIMO radar technique depends heavily on the *cross-correlation (beam)pattern* $\mathbf{a}^*(\theta)\mathbf{R}\mathbf{a}(\bar{\theta})$ (for $\theta \neq \bar{\theta}$): the said performance degrades rapidly as the cross-correlation increases (to emphasize the importance of this fact, we note that in the phased-array radar case, the probing signals at any two (different) target locations are fully correlated/coherent and, as a consequence, the standard adaptive techniques are not applicable). We will illustrate the above fact numerically in Section IV, where we apply the adaptive techniques of [6] to the data collected by a simulated MIMO radar with identically located transmit and receive antennas. Such data, under the simplifying assumption of point targets, can be described by the equation (see, e.g., [6] and [7])

$$\mathbf{y}(n) = \sum_{k=1}^{K} \beta_k \mathbf{a}^c(\theta_k)\mathbf{a}^*(\theta_k)\mathbf{x}(n) + \boldsymbol{\epsilon}(n) \tag{7}$$

where K is the number of targets that reflect the signals back to the radar receiver, $\{\beta_k\}$ are the complex amplitudes proportional to the radar-cross sections (RCSs) of those targets, $\{\theta_k\}$ are their location parameters, $\boldsymbol{\epsilon}(n)$ denotes the interference-plus-noise term, and $(\cdot)^c$ denotes the complex conjugate.

Another beampattern design problem we consider is to choose $\mathbf{R}$, under the uniform elemental power constraint in (6), to achieve the following goals.

$(\tilde{a})$ Minimize the sidelobe level in a prescribed region.

$(\tilde{b})$ Achieve a predetermined 3-dB main-beam width.

In Section IV, we will show how to formulate mathematically the goals in (a) and (b) or in $(\tilde{a})$ and $(\tilde{b})$ above, and how to solve the so-obtained design problems for $\mathbf{R}$.

Remark: The optimal designs presented in Section III, particularly those in Sections III-C and E, can be modified in a straightforward manner to accommodate other transmit power constraints, for example, a nonuniform elemental power constraint or a total transmit power constraint, $\mathrm{tr}(\mathbf{R}) = c$, where $\mathrm{tr}(\cdot)$ denotes the matrix trace. However, the constraint in (6) appears to be the most practically relevant one.

Another aspect of interest here concerns the use of equality constraints, such as (6) above, as opposed to the use of the corresponding inequality constraints, such as $R_{mm} \leq c/M$. For some of the designs presented in Sections III and IV, such as (10) with $p = M$ and (12), it is easy to show that the inequality constraint leads to the same solution as the equality constraint. On the other hand, for other designs, such as the beampattern matching design in (19) with fixed α, the weaker inequality constraint leads to a solution with a smaller matching error than that obtained with the equality constraint counterpart. However, the difference in the matching errors associated with the two said solutions is minor in many cases. More important, the power at the target locations achieved using the inequality-constraint-based design is typically smaller than that obtained using the equality-constraint-based design counterpart. Such a behavior agrees with the practical intuition that the radar should transmit at the maximum available power. For this reason and to simplify the discussions that follow, in this paper we focus on the equality constraint in (6); and leave a more detailed analysis of the differences between the designs obtained using equality and, respectively, inequality constraints for a possible future study. □

Once $\mathbf{R}$ has been determined, a signal sequence $\{\mathbf{x}(n)\}$ that has $\mathbf{R}$ as its covariance matrix can be synthesized in a number of ways. Herein we simply set $\mathbf{x}(n) = \mathbf{R}^{1/2}\mathbf{w}(n)$, where $\{\mathbf{w}(n)\}$ is a sequence of i.i.d. random vectors with mean zero and covariance matrix $\mathbf{I}$, and $\mathbf{R}^{1/2}$ denotes a square root of $\mathbf{R}$. However, we note that such a synthesizing procedure may not give a signal that satisfies all practical requirements of a real-world radar system (e.g., the above signal does not have a constant modulus). The topic of synthesizing practical probing radar signals with a given covariance matrix is left for future research (see [8] for some preliminary results on this aspect).

III. Optimal Designs

We consider four MIMO design problems in this section, that rely on no or some prior information and which employ different criteria to formulate mathematically the goals (a) and (b) or goals $(\tilde{a})$ and $(\tilde{b})$ in the previous section. The phased-array counterparts of several of the MIMO designs will be discussed as well.

To begin with, we assume that the radar has no prior information about the scene of interest.

A. Maximum Power Design For Unknown Target Locations

Let us assume that there are $\tilde{K}(\tilde{K} \leq K)$ targets of interest. Without loss of generality, they are assumed to be at locations $\{\theta_k\}_{k=1}^{\tilde{K}}$. Then the cumulated power of the probing signals at the target locations is given by

$$\sum_{k=1}^{\tilde{K}} \mathbf{a}^*(\theta_k)\mathbf{R}\mathbf{a}(\theta_k) \triangleq \mathrm{tr}(\mathbf{R}\mathbf{B}) \tag{8}$$

where

$$\mathbf{B} = \sum_{k=1}^{\tilde{K}} \mathbf{a}(\theta_k)\mathbf{a}^*(\theta_k). \tag{9}$$

In this subsection, we assume that the radar has no prior knowledge on $\mathbf{B}$. As a consequence, we can think of choosing $\mathbf{R}$ such that it maximizes (8) in the worst-case scenario

$$\begin{aligned} \max_{\mathbf{R}} \min_{\mathbf{B}} \quad & \mathrm{tr}(\mathbf{RB}) \\ \text{subject to} \quad & R_{mm} = \frac{c}{M}, \quad m = 1, \ldots, M \\ & \mathbf{R} \geq 0 \\ & \mathbf{B} \geq 0 \text{ and } \lambda_p(\mathbf{B}) \geq \varepsilon, \text{ for some } \varepsilon > 0 \\ & \text{and some } p \in [1, M] \end{aligned} \tag{10}$$

where the notation $\mathbf{R} \geq 0$ means that $\mathbf{R}$ is a positive semi-definite matrix, $\lambda_p(\mathbf{B}) \geq \varepsilon$ denotes the smallest eigenvalue of $\mathbf{B}$ that is different from zero, and the constraint $\lambda_p(\mathbf{B}) \geq \varepsilon$ is required to eliminate the trivial "solution" $\mathbf{B} = 0$ to the inner minimization.

The solution to a maximin design problem similar to (10), but with the uniform elemental power constraint $R_{mm} = c/M$, $m = 1, \ldots, M$, replaced by a less stringent total power constraint $\mathrm{tr}(\mathbf{R}) = c$, was shown in [10] to be

$$\mathbf{R} = \frac{c}{M}\mathbf{I}. \tag{11}$$

Because (11) also satisfies the uniform elemental power constraint, it is the solution to the maximin design problem in (10) as well. This solution is easy to understand intuitively: without prior information as to where the targets of interest are located, the MIMO radar will transmit a *spatially white* probing signal, which gives a constant power at any location θ, namely $(c/M)\|\mathbf{a}(\theta)\|^2 = c$ (note from (3) that $\|\mathbf{a}(\theta)\|^2 = M$, where $\|\cdot\|$ denotes the Euclidean norm).

Next we consider three design problems which assume that information about the (approximate) locations of the targets of interest is available. We will explain in due course how the said information can be obtained.

B. *Maximum Power Design for Known Target Locations*

Assume that an estimate $\hat{\mathbf{B}}$ of $\mathbf{B}$ is available. Then the inner minimization in (10) can be omitted, and the problem becomes one of maximizing the total power at the locations of the targets of interest, under the uniform elemental power constraint. While this problem is a semi-definite program (SDP) and can, therefore, be efficiently solved numerically, it does not appear to admit a closed-form solution, unlike (10). For this reason, in the following we consider the said problem but with a total power constraint instead of the elemental power one, namely

$$\begin{aligned} \max_{\mathbf{R}} \quad & \mathrm{tr}(\mathbf{R}\hat{\mathbf{B}}) \\ \text{subject to} \quad & \mathrm{tr}(\mathbf{R}) = c \\ & \mathbf{R} \geq 0. \end{aligned} \tag{12}$$

By a well-known inequality in matrix theory

$$\mathrm{tr}(\mathbf{R}\hat{\mathbf{B}}) \leq \lambda_{\max}(\hat{\mathbf{B}})\mathrm{tr}(\mathbf{R}) = c\lambda_{\max}(\hat{\mathbf{B}}) \tag{13}$$

where $\lambda_{\max}(\hat{\mathbf{B}})$ denotes the largest eigenvalue of $\hat{\mathbf{B}}$, and where the last equality follows from the constraint $\mathrm{tr}(\mathbf{R}) = c$. The upper bound in (13) is evidently achieved for

$$\mathbf{R} = c\mathbf{u}\mathbf{u}^* \tag{14}$$

where $\mathbf{u}$ is the (unit-norm) eigenvector of $\hat{\mathbf{B}}$ associated with $\lambda_{\max}(\hat{\mathbf{B}})$ (see also [10]).

Remark: For $\tilde{K} = 1$, (14) reduces to

$$\mathbf{R} = c\frac{\mathbf{a}(\hat{\theta})\mathbf{a}^*(\hat{\theta})}{\|\mathbf{a}(\hat{\theta})\|^2} \tag{15}$$

whose use leads to the delay-and-sum transmit beamformer commonly employed in phased-array radar systems. □

The maximum power design in (14) is quite simple to compute and use; in particular, the covariance matrix in (14) can be synthesized using a constant-modulus scalar signal pre-multiplied by $\mathbf{u}$. However, the design in (14) has a number of drawbacks.

1) The elemental transmit powers corresponding to (14) might vary widely.
2) While the design (14) maximizes the total power at the locations of the targets of interest, the way this power is distributed per each individual target is not controlled; consequently, the resulting powers at the target locations can be rather different from one another and from some possible desired relative levels.
3) The design (14) does not control the cross-correlation (beam)pattern either. The result is that for (14), and in fact for *any rank-one design*, the normalized magnitude of the pattern is given by (for $\theta \neq \bar{\theta}$)

$$\frac{\left|\mathbf{a}^*(\theta)\mathbf{R}\mathbf{a}(\bar{\theta})\right|}{\left[\mathbf{a}^*(\theta)\mathbf{R}\mathbf{a}(\theta)\right]^{1/2}\left[\mathbf{a}^*(\bar{\theta})\mathbf{R}\mathbf{a}(\bar{\theta})\right]^{1/2}} = \frac{\left|\mathbf{a}^*(\theta)\mathbf{u}\right|\left|\mathbf{u}^*\mathbf{a}(\bar{\theta})\right|}{\left|\mathbf{a}^*(\theta)\mathbf{u}\right|\left|\mathbf{a}^*(\bar{\theta})\mathbf{u}\right|} = 1 \tag{16}$$

(assuming that $\mathbf{u}$ is not orthogonal to either $\mathbf{a}(\theta)$ or $\mathbf{a}(\bar{\theta})$). The signals backscattered to the radar by any two targets are therefore fully coherent, which in particular makes the adaptive localization techniques inapplicable.

The next design replaces the maximum power criterion with a beampattern matching one that accommodates the uniform elemental transmit power constraint and allows the (approximate) control of the power at each target location; the new criterion also includes a term that penalizes large values of the cross-correlation (beam)pattern.

Remark: Maximizing the signal-to-interference-plus-noise ratio (SINR) at the receiver leads to a problem that has precisely the form in (10) or (12), but with a different matrix $\mathbf{B}$. To see this, note from (7) that maximizing the receiver's SINR with respect to $\mathbf{R}$ is equivalent to maximizing the following criterion:

$$\mathrm{tr}\left[\sum_{k=1}^{K}\sum_{p=1}^{K}\beta_k\beta_p^*\mathbf{a}_k^c\mathbf{a}_k^*\mathbf{R}\mathbf{a}_p\mathbf{a}_p^T\right] \triangleq \mathrm{tr}\left[\mathbf{R}\tilde{\mathbf{B}}\right] \tag{17}$$

where $\mathbf{a}_k$ is a short notation for $\mathbf{a}(\theta_k)$, and

$$\tilde{\mathbf{B}} = \sum_{k=1}^{K}\sum_{p=1}^{K}(\beta_k\beta_p^*)\left(\mathbf{a}_p^T\mathbf{a}_k^c\right)\left(\mathbf{a}_p\mathbf{a}_k^*\right) \tag{18}$$

(it can be readily checked that $\tilde{\mathbf{B}} \geq 0$). Clearly, the cost functions in (10), (12), and (18) have the same form. Furthermore, for well-separated targets (for which $\mathbf{a}_p^T \mathbf{a}_k^c \approx 0$ for $p \neq k$) with similar β_k's we have $\tilde{\mathbf{B}} \approx \mathbf{B}$ (to within a multiplicative constant).

Maximizing the SINR of the received data is presumably a more justifiable goal than maximizing the signal's power at the target locations, as in (12). Nevertheless, we focus on (12) herein, because (12) is closer than (17) to the general framework of transmit beampattern matching design of Section III-C–E; additionally, the design derived from (12), as well as the one introduced in the following, *rely only on a model for the transmit beampattern* [see (1)–(5)], whereas (17) and the corresponding design would also require the use of a model for the received data (as in (7)). □

C. Beampattern Matching Design

Let $\phi(\theta)$ denote a desired transmit beampattern, and let $\{\mu_l\}_{l=1}^{L}$ be a fine grid of points that cover the location sectors of interest. We assume that the said grid contains points which are good approximations of the locations $\{\theta_k\}_{k=1}^{\tilde{K}}$ of the targets of interest, and also like in the previous subsection, that we dispose of (initial) estimates $\{\hat{\theta}_k\}_{k=1}^{\tilde{K}}$ of $\{\theta_k\}_{k=1}^{\tilde{K}}$. We will explain how to obtain $\phi(\theta)$ and $\{\hat{\theta}_k\}_{k=1}^{\tilde{K}}$ at the end of this subsection and also in Section IV.

Our goal here is to choose $\mathbf{R}$ such that the transmit beampattern, $\mathbf{a}^*(\theta)\mathbf{R}\mathbf{a}(\theta)$, matches or rather approximates (in a least squares (LS) sense) the desired transmit beampattern, $\phi(\theta)$, over the sectors of interest, and also such that the cross-correlation (beam)pattern, $\mathbf{a}^*(\theta)\mathbf{R}\mathbf{a}(\bar{\theta})$ (for $\theta \neq \bar{\theta}$), is minimized (once again, in a LS sense) over the set $\{\hat{\theta}_k\}_{k=1}^{\tilde{K}}$. Mathematically, therefore, we want to solve the following problem:

$$\begin{aligned} \min_{\alpha,\mathbf{R}} \quad & \left\{ \frac{1}{L}\sum_{l=1}^{L} w_l \left[\alpha\phi(\mu_l) - \mathbf{a}^*(\mu_l)\mathbf{R}\mathbf{a}(\mu_l)\right]^2 \right. \\ & \left. + \frac{2w_c}{\tilde{K}^2 - \tilde{K}} \sum_{k=1}^{\tilde{K}-1} \sum_{p=k+1}^{\tilde{K}} \left|\mathbf{a}^*(\hat{\theta}_k)\mathbf{R}\mathbf{a}(\hat{\theta}_p)\right|^2 \right\} \\ \text{subject to} \quad & R_{mm} = \frac{c}{M}, \quad m = 1, \ldots, M \\ & \mathbf{R} \geq 0 \end{aligned} \tag{19}$$

where $w_l \geq 0$, $l = 1, \ldots, L$, is the weight for the lth grid point and $w_c \geq 0$ is the weight for the cross-correlation term. The value of w_l should be larger than that of w_k if the beampattern matching at μ_l is considered to be more important than the matching at μ_k. Note that by choosing $\max_l w_l > w_c$ we can give more weight to the first term in the design criterion above, and viceversa for $\max_l w_l < w_c$.

The above criterion appears to improve, in several ways, over a related design criterion used in [3] (the more recent paper [8] has also proposed a minmax version of the least-squares criterion in [3], which however did not offer any clear improvement of performance and which will not be considered in this paper).

- The LS fitting in [3] is done to $\phi^{1/2}(\theta)$, for computational reasons; fitting directly to $\phi(\theta)$, as in (19), is more natural (this problem has been fixed in the recent full version [8] of [3]).
- In [3], the scaling factor α is determined in a suboptimal manner, prior to the fitting of the beampattern, whereas in (19) α is obtained optimally as part of the solution to the LS matching problem. The reason for introducing α in the design problem is that typically $\phi(\theta)$ is given in a "normalized form" (e.g., satisfying $\phi(\theta) \leq 1, \forall\theta$), and our interest lies in approximating an appropriately scaled version of $\phi(\theta)$, not $\phi(\theta)$ itself.
- The need to penalize large values of the cross-correlation pattern was not recognized in [3], and thus the second term in (19) did not appear in the criterion used in the cited reference.

Additionally, as explained below, we show that the design problem (19) can be *efficiently solved in polynomial time* as a SQP; in contrast to this, [3] used a rather inefficient gradient-based algorithm to minimize the related criterion considered there (the recent full version [8] of [3] also considers the use of a convex optimization algorithm, albeit less efficient than the SQP algorithm proposed here, for solving the signal design problem). We also explain how the prior information needed to define (19) can be obtained, an aspect that was not addressed in [3].

To show that the problem (19) is a SQP, we need some additional notation. Let $\mathrm{vec}(\mathbf{R})$ denote the $M^2 \times 1$ vector obtained by stacking the columns of $\mathbf{R}$ on top of each other. Let $\mathbf{r}$ denote the $M^2 \times 1$ real-valued vector made from R_{mm} $(m = 1, \ldots, M)$ and the real and imaginary parts of R_{mp}, $(m, p = 1, \ldots, M; p > m)$. Then, given the Hermitian symmetry of $\mathbf{R}$, we can write

$$\mathrm{vec}(\mathbf{R}) = \mathbf{J}\mathbf{r} \tag{20}$$

for a suitable $M^2 \times M^2$ matrix $\mathbf{J}$ whose elements are easily derived constants $(0, \pm j, \pm 1)$. Making use of (20) and of some simple properties of the vec operator, the reader can verify that (the symbol $\otimes$ denotes the Kronecker product operator)

$$\begin{aligned} \mathbf{a}^*(\mu_l)\mathbf{R}\mathbf{a}(\mu_l) &= \mathrm{vec}\left[\mathbf{a}^*(\mu_l)\mathbf{R}\mathbf{a}(\mu_l)\right] \\ &= \left[\mathbf{a}^T(\mu_l) \otimes \mathbf{a}^*(\mu_l)\right]\mathbf{J}\mathbf{r} \\ &\triangleq -\mathbf{g}_l^T\mathbf{r} \end{aligned} \tag{21}$$

and

$$\begin{aligned} \mathbf{a}^*(\hat{\theta}_k)\mathbf{R}\mathbf{a}(\hat{\theta}_p) &= \left[\mathbf{a}^T(\hat{\theta}_p) \otimes \mathbf{a}^*(\hat{\theta}_k)\right]\mathbf{J}\mathbf{r} \\ &\triangleq \mathbf{d}_{k,p}^*\mathbf{r}. \end{aligned} \tag{22}$$

Inserting (21) and (22) into (19) yields the following more compact form of the design criterion (which shows clearly the quadratic dependence on $\mathbf{r}$ and α)

$$\begin{aligned} & \frac{1}{L}\sum_{l=1}^{L} w_l \left[\alpha\phi(\mu_l) + \mathbf{g}_l^T\mathbf{r}\right]^2 \\ & + \frac{2w_c}{\tilde{K}^2 - \tilde{K}} \sum_{k=1}^{\tilde{K}-1} \sum_{p=k+1}^{\tilde{K}} \left|\mathbf{d}_{k,p}^*\mathbf{r}\right|^2 \\ & = \frac{1}{L}\sum_{l=1}^{L} w_l \left\{ \begin{bmatrix} \phi(\mu_l) & \mathbf{g}_l^T \end{bmatrix} \begin{bmatrix} \alpha \\ \mathbf{r} \end{bmatrix} \right\}^2 \\ & \quad + \frac{2w_c}{\tilde{K}^2 - \tilde{K}} \sum_{k=1}^{\tilde{K}-1} \sum_{p=k+1}^{\tilde{K}} \left| \begin{bmatrix} 0 & \mathbf{d}_{k,p}^* \end{bmatrix} \begin{bmatrix} \alpha \\ \mathbf{r} \end{bmatrix} \right|^2 \\ & \triangleq \boldsymbol{\rho}^T\boldsymbol{\Gamma}\boldsymbol{\rho}, \end{aligned} \tag{23}$$

where

$$\boldsymbol{\rho} = \begin{bmatrix} \alpha \\ \mathbf{r} \end{bmatrix} \tag{24}$$

and

$$\boldsymbol{\Gamma} = \frac{1}{L}\sum_{l=1}^{L} w_l \begin{bmatrix} \phi(\mu_l) \\ \mathbf{g}_l \end{bmatrix} [\, \phi(\mu_l) \quad \mathbf{g}_l^T \,] + \mathrm{Re}\left\{ \frac{2w_c}{\tilde{K}^2 - \tilde{K}} \sum_{k=1}^{\tilde{K}-1} \sum_{p=k+1}^{\tilde{K}} \begin{bmatrix} 0 \\ \mathbf{d}_{k,p} \end{bmatrix} [\, 0 \quad \mathbf{d}_{k,p}^* \,] \right\} \tag{25}$$

with $\mathrm{Re}(\cdot)$ denoting the real part. The matrix $\boldsymbol{\Gamma}$ above is usually rank deficient. For example, in the case of an M-sensor uniform linear array with half-wavelength or smaller inter-element spacing and for $w_c = 0$, one can show that the rank of $\boldsymbol{\Gamma}$ is $2M$. The rank deficiency of $\boldsymbol{\Gamma}$, however, does not pose any serious problem for the SQP solver outlined below.

Making use of the form in (23) of the design criterion, we can rewrite (19) as the following SQP (see, e.g., [11], [12]):

$$\begin{aligned} \min_{\delta, \boldsymbol{\varrho}} \quad & \delta \\ \text{subject to} \quad & \|\boldsymbol{\varrho}\| \le \delta \\ & R_{mm}(\boldsymbol{\varrho}) = \frac{c}{M}, \quad m = 1, \ldots, M \\ & \mathbf{R}(\boldsymbol{\varrho}) \ge 0 \end{aligned} \tag{26}$$

where ($\boldsymbol{\Gamma}^{1/2}$ denotes a square root of $\boldsymbol{\Gamma}$)

$$\boldsymbol{\varrho} = \boldsymbol{\Gamma}^{1/2}\boldsymbol{\rho} \tag{27}$$

and where we have indicated explicitly the (linear) dependence of $\mathbf{R}$ on $\boldsymbol{\varrho}$. For practical values of the array size M, the SQP above can be efficiently solved on a personal computer using public domain software (e.g., [11]).

In some applications, we would like that the synthesized beampattern at some given locations be very close to the desired values. As already mentioned, to a certain extent, this design goal can be achieved by the selection of the weights $\{w_l\}$ of the design criterion in (19). However, if we want the beampattern to match the desired values *exactly*, then selecting the weights $\{w_l\}$ is not enough and we have to modify the design problem as we now explain.

Consider, for instance, that we want the transmit beampattern at a number of points to be equal to certain desired levels. Then the optimization problem we need to solve is (19) with the following additional constraints:

$$\mathbf{a}^*(\breve{\mu}_l)\mathbf{R}\mathbf{a}(\breve{\mu}_l) = \zeta_l, \quad l = 1, \ldots, \breve{L} \tag{28}$$

where $\{\zeta_l\}$ are predetermined levels. A similar modification of (19) takes place when the transmit beampattern at a number of points $\{\breve{\mu}_l\}_{l=1}^{\breve{L}}$ is restricted to be less than or equal to certain desired levels. The extended problems (with additional either equality or inequality constraints) are also SQP's, and therefore, similarly to (19), they can be solved efficiently using readily available software [11], [12].

To conclude this subsection, we explain briefly how the desired transmit beampattern, $\phi(\theta)$, and the (initial) location estimates can be obtained (this aspect is further discussed in Section IV). Because at the beginning of the operation, the MIMO radar system is assumed to have no prior knowledge of the scene, we transmit a maximin power optimal signal towards the targets, for which $\mathbf{R} = (c/M)\mathbf{I}$ (see (11)). Using the data $\mathbf{y}(n)_{n=1}^N$ collected by the receiving array of the system, we then compute the generalized likelihood ratio test (GLRT) function in [6], which is given by

$$\tilde{\phi}(\theta) = 1 - \frac{\mathbf{a}^*(\theta)\hat{\mathbf{R}}_{yy}^{-1}\mathbf{a}(\theta)}{\mathbf{a}^*(\theta)\hat{\mathbf{Q}}^{-1}\mathbf{a}(\theta)} \tag{29}$$

where

$$\hat{\mathbf{Q}} = \hat{\mathbf{R}}_{yy} - \frac{\hat{\mathbf{R}}_{yx}\mathbf{a}(\theta)\mathbf{a}^*(\theta)\hat{\mathbf{R}}_{yx}^*}{\mathbf{a}^*(\theta)\hat{\mathbf{R}}_{xx}\mathbf{a}(\theta)} \tag{30}$$

with

$$\hat{\mathbf{R}}_{yx} = \frac{1}{N}\sum_{n=1}^{N} \mathbf{y}(n)\mathbf{x}^*(n) \tag{31}$$

and $\hat{\mathbf{R}}_{xx}$ and $\hat{\mathbf{R}}_{yy}$ similarly defined. (Note that, while $\mathbf{R} = (c/M)\mathbf{I}$, the sample matrix $\hat{\mathbf{R}}_{xx}$ will in general be somewhat different from $(c/M)\mathbf{I}$.) The above function $\tilde{\phi}(\theta)$ possesses the following useful properties (see [6] for details).

1) It has values close to one in the vicinity of the target locations $\{\theta_k\}_{k=1}^K$, and close to zero elsewhere.
2) Unlike the spatial (pseudo)spectra obtained with other methods, (29) takes on small values even at the locations of possibly strong jammers (assuming that the jamming signals are uncorrelated with $\mathbf{x}(n)$).
3) The peaks of (29) around the target locations have widths that lead to a good compromise between resolution and robustness.

With the above features in mind, we can use the locations of interest of the dominant peaks of $\tilde{\phi}(\theta)$ as estimates of $\{\theta_k\}_{k=1}^{\tilde{K}}$ and also to obtain a desired transmit beampattern—see Section IV for details. Note that, in view of the features above, the MIMO radar will not waste power by probing either jammer locations (which may have the added bonus of making the radar harder to detect) or locations of uninteresting targets (which allows the radar to transmit spatially more power towards the targets of interest).

D. Minimum Sidelobe Beampattern Design

In some applications, the beampattern design goal is to minimize the sidelobe level in a certain sector, when pointing the MIMO radar toward θ_0 (let us say). Such a minimum sidelobe beampattern design problem, with the uniform elemental transmit power constraint, can be formulated as follows:

$$\begin{aligned} \min_{t, \mathbf{R}} \quad & -t \\ \text{subject to} \quad & \mathbf{a}^*(\theta_0)\mathbf{R}\mathbf{a}(\theta_0) - \mathbf{a}^*(\mu_l)\mathbf{R}\mathbf{a}(\mu_l) \ge t, \quad \forall \mu_l \in \Omega \\ & \mathbf{a}^*(\theta_1)\mathbf{R}\mathbf{a}(\theta_1) = 0.5\mathbf{a}^*(\theta_0)\mathbf{R}\mathbf{a}(\theta_0) \\ & \mathbf{a}^*(\theta_2)\mathbf{R}\mathbf{a}(\theta_2) = 0.5\mathbf{a}^*(\theta_0)\mathbf{R}\mathbf{a}(\theta_0) \\ & \mathbf{R} \ge 0 \\ & R_{mm} = \frac{c}{M}, \quad m = 1, \ldots, M \end{aligned} \tag{32}$$

where $\theta_2 - \theta_1$ (with $\theta_2 > \theta_0$ and $\theta_1 < \theta_0$) determines the 3 dB main-beam width and Ω is a discrete set that covers the sidelobe

region of interest. This is a SDP that can be solved in polynomial time using public domain software (e.g., [11]). Similarly to the optimal SQP-based design of the previous subsection, if desired, the elemental power constraint can be replaced by a total power constraint. Note that we can relax somewhat the constraints in (32) defining the 3 dB main-beam width; for instance, we can replace them by $(0.5-\delta)\mathbf{a}^*(\theta_0)\mathbf{R}\mathbf{a}(\theta_0) \leq \mathbf{a}^*(\theta_i)\mathbf{R}\mathbf{a}(\theta_i) \leq (0.5+\delta)\mathbf{a}^*(\theta_0)\mathbf{R}\mathbf{a}(\theta_0)$, $i=1,2$, for some small δ. Such a relaxation leads to a design with lower sidelobes, and to an optimization problem that is feasible more often than (32).

We can also introduce some flexibility in the elemental power constraint by allowing the elemental power to be within a certain range around c/M, while still maintaining the same total transmit power of c. Such a relaxation of the design problem allows lower sidelobe levels and smoother beampatterns, as we will show later on via some numerical examples.

E. Phased-Array Beampattern Designs

Finally, we comment on the conventional phased-array beampattern design problem in which only the array weight vector can be adjusted and therefore all antennas transmit the same differently scaled waveform. We can readily modify the previously described beampattern matching or minimum sidelobe beampattern designs for the case of phased-arrays by adding the constraint

$$\mathrm{rank}(\mathbf{R}) = 1 \tag{33}$$

to (19) or (32), respectively, (other phased-array designs proposed in the literature, see e.g., [13] and [14], are rather different from (19) or (32) with (33), and they will not be considered in this paper). However, due to the rank-one constraint, both these originally convex optimization problems become nonconvex. The lack of convexity makes the rank-one constrained problems much harder to solve than the original convex optimization problems [15]. Semi-definite relaxation (SDR) is often used to obtain approximate solutions to such rank-constrained optimization problems [12]. The SDR is obained by omitting the rank constraint. Hence, interestingly, *the MIMO beampattern design problems are the SDRs of the corresponding phased-array beampattern design problems*.

In the numerical examples of Section IV, we have used the Newton-like algorithm presented in [15] to solve the rank-one constrained design problems for phased-arrays. The said algorithm uses SDR to obtain an initial solution, which is the exact solution to the corresponding MIMO beampattern design problem. Although the convergence of the Newton-like algorithm is not guaranteed [15], we did not encounter any apparent problem in our simulations (we have started the algorithm from different initial solutions, including the all-zero vector, and observed no significant difference between the "final" solutions so obtained). An interesting detail here is that the approach in [15] is for real-valued vectors and matrices; therefore we had to re-write the rank-one constraint in (33) in terms of real-valued quantities

$$\mathrm{rank}(\tilde{\mathbf{R}}) = 2 \tag{34}$$

where

$$\tilde{\mathbf{R}} = \begin{bmatrix} \mathrm{Re}\{\mathbf{R}\} & -\mathrm{Im}\{\mathbf{R}\} \\ \mathrm{Im}\{\mathbf{R}\} & \mathrm{Re}\{\mathbf{R}\} \end{bmatrix} \tag{35}$$

with $\mathrm{Re}\{\mathbf{x}\}$ and $\mathrm{Im}\{\mathbf{x}\}$ denoting the real and imaginary parts of $\mathbf{x}$, respectively. The equivalence between (33) and (34) is proven in the Appendix.

IV. Numerical Examples

We present several numerical examples to demonstrate the merits of the proposed probing signal designs for MIMO radar systems. We consider a MIMO radar with a uniform linear array (ULA) comprising $M=10$ antennas with half-wavelength spacing between adjacent antennas. The said array is used both for transmitting and for receiving. Without loss of generality, the total transmit power is set to $c=1$.

A. Beampattern Matching Design

Consider first a scenario where $K=3$ targets are located at $\theta_1=-40^\circ$, $\theta_2=0^\circ$, and $\theta_3=40^\circ$ with complex amplitudes equal to $\beta_1=\beta_2=\beta_3=1$. There is a strong jammer at 25° with an unknown waveform (uncorrelated with the transmitted MIMO radar waveforms) with a power equal to 10^6 (60 dB). Each transmitted signal pulse has $N=256$ samples. The received signal is corrupted by zero-mean circularly symmetric spatially and temporally white Gaussian noise with variance σ^2. We assume that only the targets reflect the transmitted signals. In practice, the background can also reflect the signals. In the latter case, transmitting most of the power towards the targets should generate much less clutter returns than when transmitting power omnidirectionally. Therefore, a MIMO radar system with a proper transmit beampattern design might provide even larger performance gains than those demonstrated herein.

Since we do not assume any prior knowledge about the target locations, the initial probing relies on the maximum power beampattern design for unknown target locations, i.e., $\mathbf{R}=(c/M)\mathbf{I}$. The corresponding transmit beampattern is omnidirectional with power equal to $c=1$ at any θ. Using the data collected as a result of this initial probing, the target locations can be estimated using the GLRT technique, (29)–(31), outlined in the previous section. Alternatively, location estimates can be obtained using the Capon technique, as the maximum points of the following spatial spectrum (see [6] for details):

$$\frac{\left|\mathbf{a}^*(\theta)\hat{\mathbf{R}}_{yy}^{-1}\hat{\mathbf{R}}_{yx}\mathbf{a}^c(\theta)\right|}{\left[\mathbf{a}^*(\theta)\hat{\mathbf{R}}_{yy}^{-1}\mathbf{a}(\theta)\right]\left[\mathbf{a}^T(\theta)\hat{\mathbf{R}}_{xx}\mathbf{a}^c(\theta)\right]}. \tag{36}$$

An example of the Capon spectrum for $\sigma^2=-10$ dB is shown in Fig. 1(a), where very narrow peaks occur around the target locations. Note that in Fig. 1(a), a false peak occurs around $\theta=25^\circ$ due to the presence of the very strong jammer. The corresponding GLRT pseudo-spectrum as a function of θ is shown in Fig. 1(b). Note that the GLRT is close to one at the target locations and close to zero at any other locations including the jammer location. Therefore, the GLRT can be used to reject the

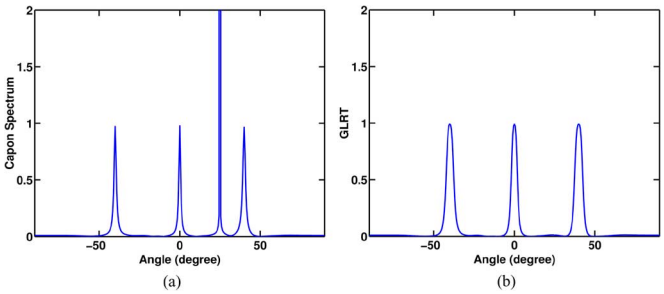

Fig. 1. Capon spatial spectrum and the GLRT pseudo-spectrum as functions of θ, for the initial omnidirectional probing. (a) Capon. (b) GLRT.

jammer peak in the Capon spectrum. The remaining peak locations in the Capon spectrum are the estimated target locations. Note that the Capon spectrum has sharper peaks than the GLRT function and hence, if desired, we can use the Capon estimates of the target locations in lieu of the GLRT estimates.

The initial target locations obtained by Capon or by GLRT can be used to compute the maximum power design in (14); we will use the GLRT estimates in what follows. An example of the transmit beampattern synthesized using the so-obtained $\mathbf{R}$ is shown in Fig. 2(a). Since the rank of $\mathbf{R}$ is equal to one for this design, the MIMO radar operates as a conventional phased-array radar in this case. As a consequence, in the presence of multiple targets, no data-adaptive approach can be used to obtain enhanced estimates of the target locations since the signals reflected by the targets are coherent with each other.

The initial target location estimates obtained using Capon or the GLRT can also be used to derive a desired beampattern for the beampattern matching design. In the following numerical examples, we form the desired beampattern by using the dominant peak locations of the GLRT pseudo-spectrum, denoted as $\hat{\theta}_1, \cdots, \hat{\theta}_{\hat{K}}$, as follows (with $\hat{K}$ being the resulting estimate of K):

$$\phi(\theta) = \begin{cases} 1, & \theta \in [\hat{\theta}_k - \Delta, \hat{\theta}_k + \Delta],\ k = 1, \ldots, \hat{K} \\ 0, & \text{otherwise} \end{cases} \tag{37}$$

where 2Δ is the chosen beamwidth for each target (Δ should be greater than the expected error in $\{\hat{\theta}_k\}$). Fig. 2(b) is obtained using $\Delta = 10^\circ$ in the beampattern matching design in (19) with a mesh grid size of 0.1°, $w_l = 1, l = 1, \ldots, L$, and $w_c = 0$. The dashed line shows the desired beampattern in (37) scaled by the optimal value of α. Fig. 2(c) shows the corresponding optimal phased-array beampattern (obtained using the additional constraint $\mathrm{rank}(\mathbf{R}) = 1$). Note that the phased-array beampattern has higher sidelobe levels than its MIMO counterpart. Also, note that the synthesized MIMO transmit beampattern is symmetric (or nearly so), which is quite natural in view of the fact that the desired pattern is symmetric, whereas the optimal phased-array beampattern is asymmetric (generating a symmetric pattern with a phased-array would worsen the matching performance significantly). More importantly, in the presence of multiple targets, even though phased-arrays can be used to form a transmit beampattern with peaks at the target locations, no data-adaptive approach can be used for localization or detection purposes since the signals reflected by the targets are coherent with each other.

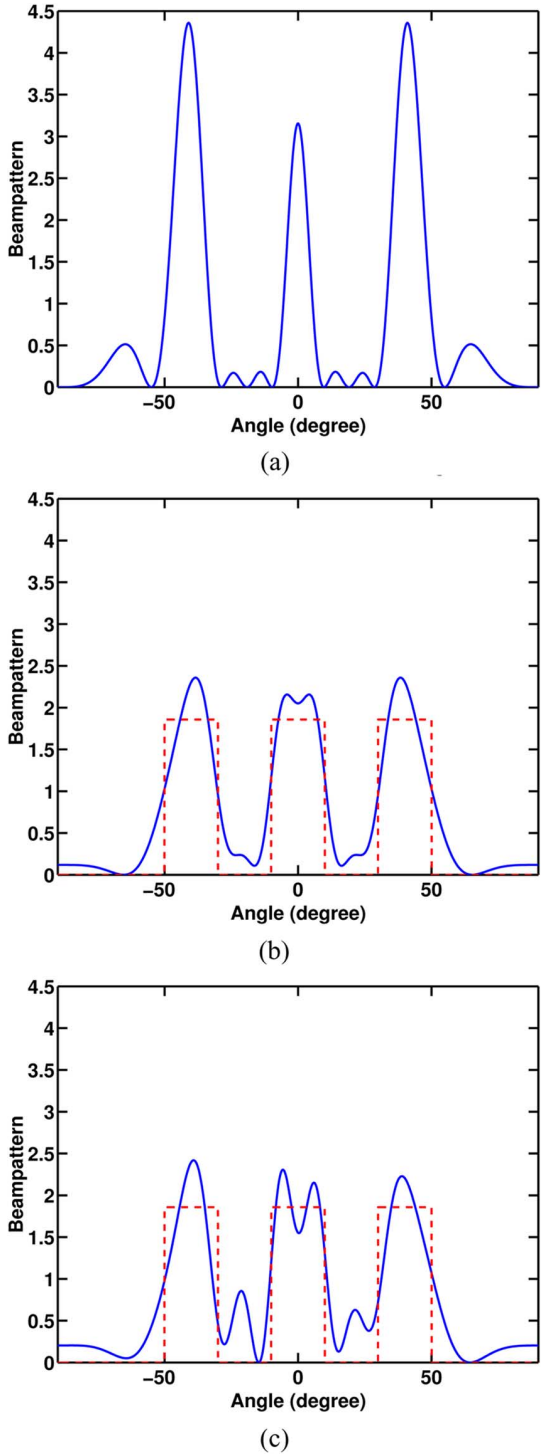

Fig. 2. Transmit beampatterns formed via (a) maximum power design for given target locations (estimated via initial omnidirectional probing), (b) MIMO beampattern matching design with $w_c = 0$ under the uniform elemental power constraint when $\Delta = 10^\circ$, and (c) phased-array beampattern matching design with $w_c = 0$ under the uniform elemental power constraint when $\Delta = 10^\circ$. The desired beampatterns (scaled by α) for (b) and (c) are shown by dashed lines.

Note that although we used $w_c = 0$ to obtain Fig. 2(b), we have found out that the signals reflected by the targets exhibit low cross-correlations among them. As Δ is decreased, however, the cross-correlations become stronger when $w_c = 0$; consequently to achieve low cross-correlations in such a case, we

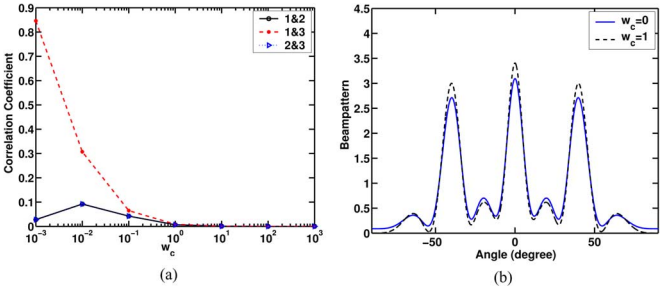

Fig. 3. MIMO beampattern matching designs with $\Delta = 5^\circ$ under the uniform elemental power constraint. (a) Cross-correlation coefficients of the three target reflected signals as functions of w_c. (b) Comparison of the beampatterns obtained with $w_c = 0$ and $w_c = 1$.

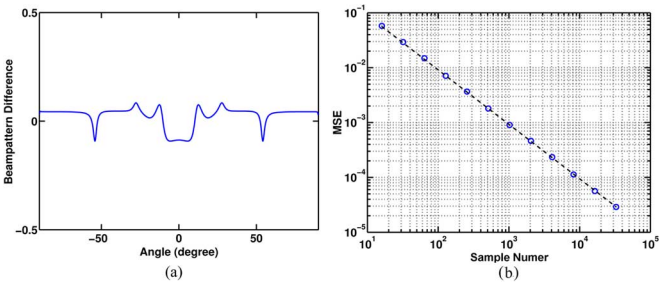

Fig. 4. Analysis of the beampattern difference resulting from using $\hat{\mathbf{R}}_{xx}$ in lieu of $\mathbf{R}$. (a) Beampattern difference versus θ when $N = 256$. (b) Average MSE of the beampattern difference as a function of the sample number N.

need to increase the weight of the second term of the cost function in (19). The normalized magnitudes of the cross-correlation coefficients of the target reflected signals, as functions of w_c, are shown in Fig. 3(a) for $\Delta = 5^\circ$. We note that when w_c is close to zero, the first and third reflected signals are highly correlated, which can degrade significantly the performance of any adaptive technique. For $w_c = 1$, on the other hand, all cross-correlation coefficients are approximately zero. An example of the beampattern obtained with $w_c = 1$ is shown in Fig. 3(b), where it is compared with the corresponding beampattern obtained with $w_c = 0$. Note that the designs obtained with $w_c = 1$ and with $w_c = 0$ are similar to one another even though the cross-correlation behavior of the former is much better than that of the latter.

In practice, the theoretical covariance matrix $\mathbf{R}$ of the transmitted signals is realized via the sample covariance matrix $\hat{\mathbf{R}}_{xx} = 1/N \sum_{n=1}^{N} \mathbf{x}(n)\mathbf{x}^*(n)$, which may cause the synthesized transmit beampattern to be slightly different from the designed beampattern (unless $\hat{\mathbf{R}}_{xx} = \mathbf{R}$, which holds for instance if $\mathbf{x}(n) = \mathbf{R}^{1/2}\mathbf{w}(n)$ and $1/N \sum_{n=1}^{N} \mathbf{w}(n)\mathbf{w}^*(n) = \mathbf{I}$ exactly; in what follows, however, we assume that $\{\mathbf{w}(n)\}$ is a temporally and spatially white signal from which the last equality holds only approximately in finite samples). Let $\epsilon(\theta)$ denote the relative difference of the beampatterns obtained by using $\hat{\mathbf{R}}_{xx}$ and $\mathbf{R}$

$$\epsilon(\theta) = \frac{\mathbf{a}^*(\theta)(\hat{\mathbf{R}}_{xx} - \mathbf{R})\mathbf{a}(\theta)}{\mathbf{a}^*(\theta)\mathbf{R}\mathbf{a}(\theta)}, \quad \theta \in [-90^\circ, 90^\circ]. \tag{38}$$

Fig. 4(a) shows an example of $\epsilon(\theta)$, as a function of θ, for the beampattern design in Fig. 3(b) with $w_c = 1$ and for $N = 256$. Note that the difference is quite small. We define the

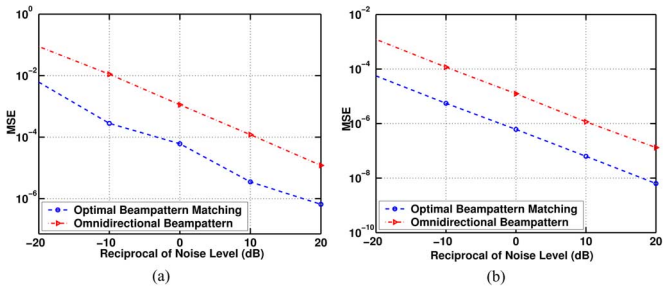

Fig. 5. MSEs of (a) the location estimates and of (b) the complex amplitude estimates for the first target, as functions of $-10 \log_{10} \sigma^2$, obtained with initial omnidirectional probing and with probing using the beampattern matching design with $\Delta = 5^\circ$ and $w_c = 1$, under the uniform elemental power constraint.

mean-squared error (MSE) between the beampatterns obtained by using $\hat{\mathbf{R}}_{xx}$ and $\mathbf{R}$ as the average of the square of (38) over all mesh grid points and over the set of Monte Carlo trials. The MSE as a function of N, obtained from 1000 Monte Carlo trials, is shown in Fig. 4(b). As expected, the larger the sample number N, the smaller the MSE.

Next, we consider estimating the complex amplitudes $\{\beta_k\}$ of the reflected signals, (see (7)), in addition to estimating their location parameters $\{\theta_k\}$. We recommend using the approximate maximum likelihood (AML) approach of [16] to estimate the amplitude vector $\boldsymbol{\beta} = [\beta_1 \quad \dots \quad \beta_{\hat{K}}]^T$. Let $\{\hat{\theta}_k\}_{k=1}^{\hat{K}}$ denote the estimated target locations and let

$$\mathbf{A} = [\mathbf{a}(\hat{\theta}_1) \quad \dots \quad \mathbf{a}(\hat{\theta}_{\hat{K}})]. \tag{39}$$

Then

$$\hat{\boldsymbol{\beta}}_{\mathrm{AML}} = [(\mathbf{A}^T\mathbf{T}^{-1}\mathbf{A}^c) \odot (\mathbf{A}^T\hat{\mathbf{R}}_{xx}^c\mathbf{A}^c)]^{-1} \mathrm{vecd}(\mathbf{A}^T\mathbf{T}^{-1}\hat{\mathbf{R}}_{yx}\mathbf{A}) \tag{40}$$

where $\odot$ denotes the Hadamard product, $\mathrm{vecd}(\cdot)$ denotes a column vector formed by the diagonal elements of a matrix, and

$$\mathbf{T} = \hat{\mathbf{R}}_{yy} - \hat{\mathbf{R}}_{yx}\mathbf{A}(\mathbf{A}^*\hat{\mathbf{R}}_{xx}\mathbf{A})^{-1}\mathbf{A}^*\hat{\mathbf{R}}_{yx}^*. \tag{41}$$

We examine the MSEs of the location estimates obtained by Capon and of the complex amplitude estimates obtained by AML. In particular, we compare the MSEs obtained using the initial omnidirectional probing with those obtained using the optimal beampattern matching design shown in Fig. 3(b) with $\Delta = 5^\circ$ and w_c=1. Fig. 5(a) and (b) shows the MSE curves of the location and complex amplitude estimates obtained for the first target from 1000 Monte Carlo trials (the results for the other targets are similar). The estimates obtained using the optimal beampattern matching design are much better: the SNR gain over the omnidirectional design is larger than 10 dB.

Consider now an example where two of the targets are closely spaced. We assume that there are $K = 3$ targets, located at $\theta_1 = -40^\circ$, $\theta_2 = 0^\circ$, and $\theta_3 = 3^\circ$ with complex amplitudes equal to $\beta_1 = \beta_2 = \beta_3 = 1$. There is a strong jammer at 25° with an unknown waveform, which is uncorrelated with the transmitted MIMO radar waveforms, and with a power equal to 10^6 (60 dB). Each transmitted signal pulse has $N = 256$ samples. The received signal is corrupted by zero-mean circularly symmetric spatially and temporally white Gaussian noise with

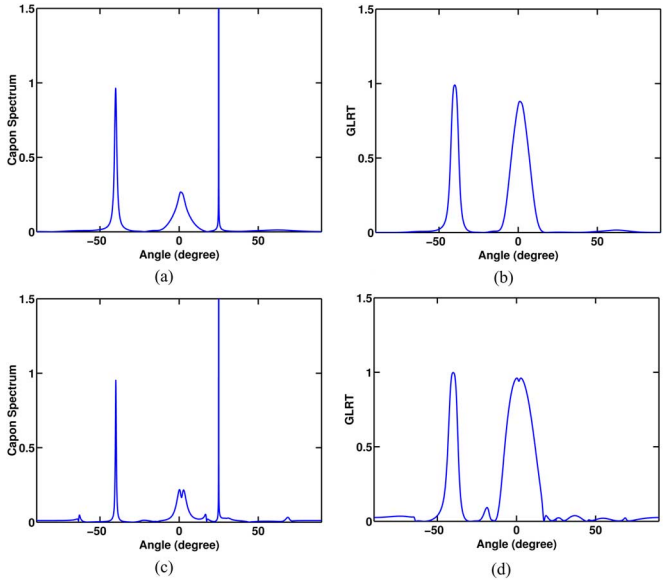

Fig. 6. Capon spatial spectra and the GLRT pseudo-spectra as functions of θ. (a) Capon for the initial omnidirectional probing. (b) GLRT for the initial omnidirectional probing. (c) Capon for the optimal probing. (d) GLRT for the optimal probing.

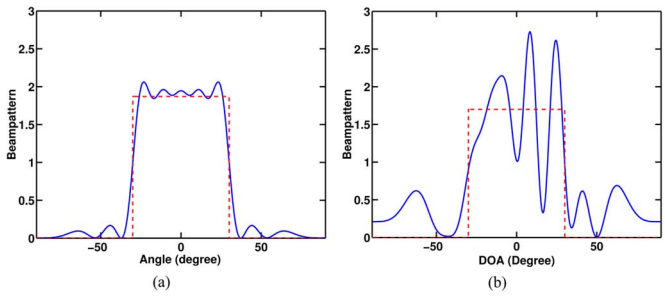

Fig. 7. Beampattern matching designs under the uniform elemental power constraint. (a) MIMO. (b) Phased-array.

variance $\sigma^2 = -10$ dB. Fig. 6(a) and (b) shows the Capon spectrum and the GLRT pseudo-spectrum, respectively, for the initial omnidirectional probing; as can be seen from these figures, the two closely spaced targets cannot be resolved. Using this initial probing result, we derive an optimal beampattern matching design using (19) with a mesh grid size of 0.1°, $w_l = 1$, $l = 1, \ldots, L$, and $w_c = 1$. Since the initial probing indicated only two dominant peaks, these two peak locations are used in (19). The desired beampattern is given by (37) with $\Delta = 10°$ and $\hat{K} = 2$. Fig. 6(c) and (d), respectively, show the Capon spectrum and the GLRT pseudo-spectrum for the optimal probing. In principle, the two closely spaced targets are now resolved.

To conclude this subsection, we consider an example where the desired beampattern has only one wide beam centered at 0° with a width of 60°. Fig. 7(a) shows the result for the beampattern matching design in (19) with a mesh grid size of 0.1°, $w_l = 1$, $l = 1, \ldots, L$, and $w_c = 0$. Fig. 7(b) shows the corresponding phased-array beampattern obtained by using the additional constraint of $\mathrm{rank}(\mathbf{R}) = 1$ in (19). We note that, under the elemental power constraint, the number of degrees of freedom (DOF) of the phased-array that can be used for beampattern design is equal to only $M - 1$ (real-valued parameters); consequently, it is difficult for the phased-array to synthesize a proper wide beam. The MIMO design, however, can be used to achieve a beampattern significantly closer to the desired beampattern due to its much larger number of DOF, viz. $M^2 - M$. Interestingly, we have observed in a number of cases that, under the total power constraint, the optimal MIMO beampattern and the optimal phased-array beampattern were quite close to one another (it is unknown whether this holds in general or not). The elemental powers of the phased-array design obtained under the total power constraint, however, varied significantly, which may be undesirable in many applications.

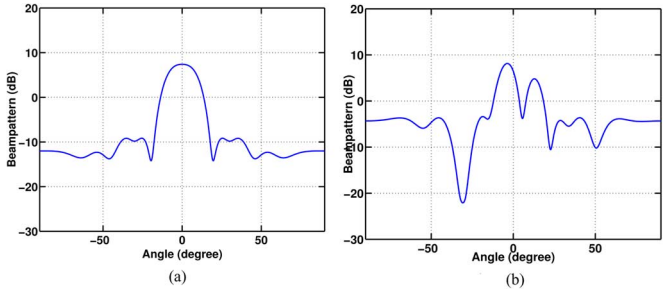

Fig. 8. Minimum sidelobe beampattern designs, under the uniform elemental power constraint, when the 3 dB main-beam width is 20°. (a) MIMO. (b) Phased-Array.

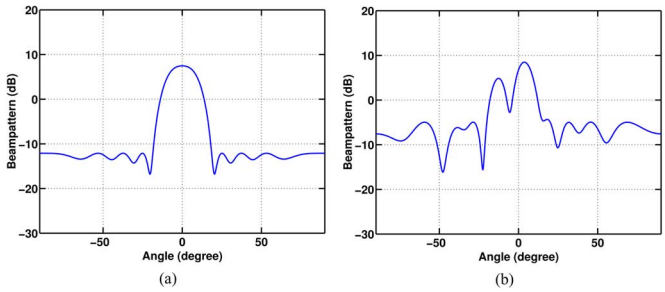

Fig. 9. Minimum sidelobe beampattern designs, under a relaxed ($\pm 20\%$) elemental power constraint, when the 3 dB main-beam width is 20°. (a) MIMO. (b) Phased-Array.

B. Minimum Sidelobe Beampattern Design

Consider the beampattern design problem in (32) with the main-beam centered at $\theta_0 = 0°$ and with a 3 dB width equal to 20° ($\theta_1 = -10°$, $\theta_2 = 10°$). The sidelobe region is $\Omega = [-90°, -20°] \cup [20°, 90°]$. The minimum-sidelobe beampattern design obtained by using (32) with a mesh grid size of 0.1° is shown in Fig. 8(a). Note that the peak sidelobe level achieved by the MIMO design is approximately 18 dB below the mainlobe peak level. Fig. 8(b) shows the corresponding phased-array beampattern obtained by using the additional constraint $\mathrm{rank}(\mathbf{R}) = 1$ in (32). The phased-array design fails to provide a proper mainlobe (it suffers from peak splitting) and its peak sidelobe level is about 5 dB higher than that of its MIMO counterpart.

Fig. 9 is similar to Fig. 8 except that now we allow the elemental powers to be between 80% and 120% of $c/M = 1/10$, while the total power is still constrained to be $c = 1$. Observe that by allowing such a flexibility in setting the elemental powers, we can bring down the peak sidelobe level of the MIMO

beampattern by about 3 dB. The phased-array design, on the other hand, does not appear to improve in any significant way.

V. Conclusion

We have considered several transmit beampattern design problems for MIMO radar systems. We have shown that through beampattern design, by focusing the transmit power around the locations of the targets of interest while minimizing the cross-correlations of the signals reflected back to the radar, we can significantly improve the parameter estimation accuracy of the adaptive MIMO radar techniques as well as enhance their resolution. We have also shown that, due to the significantly larger number of degrees of freedom of a MIMO system, we can achieve much better transmit beampatterns under the practical uniform elemental transmit power constraint with a MIMO radar than with its phased-array counterpart.

Appendix

Lemma: Let $\mathbf{R} \in \mathcal{C}^{M\times M}$, and let $\tilde{\mathbf{R}} \in \mathcal{R}^{2M\times 2M}$ be as defined in (35). Then

$$\operatorname{rank}(\mathbf{R}) = M - m \Longleftrightarrow \operatorname{rank}(\tilde{\mathbf{R}}) = 2(M-m), \quad \text{for } m = 0,\ldots,M. \tag{42}$$

Proof: Let $\mathbf{v} \in \mathcal{C}^{M\times 1}$, $\mathbf{v} \neq 0$, be a vector in the null space of $\mathbf{R}$, $\mathcal{N}(\mathbf{R})$, i.e.,

$$\mathbf{R}\mathbf{v} = 0. \tag{43}$$

This implies that

$$\tilde{\mathbf{R}}\,[\operatorname{Re}\{\mathbf{v}^T\}\ \operatorname{Im}\{\mathbf{v}^T\}]^T = 0. \tag{44}$$

Moreover, since (43) also implies $\mathbf{R}(j\mathbf{v}) = 0$, we must also have

$$\tilde{\mathbf{R}}\,[-\operatorname{Im}\{\mathbf{v}^T\}\ \operatorname{Re}\{\mathbf{v}^T\}]^T = 0. \tag{45}$$

The vectors appearing in (44) and (45) are linearly independent of each other. Indeed, if we assume that they were not, then there would exist a nonzero complex-valued scalar, say $\zeta \neq 0$, such that

$$\begin{bmatrix} \operatorname{Re}\{\mathbf{v}\} & -\operatorname{Im}\{\mathbf{v}\} \\ \operatorname{Im}\{\mathbf{v}\} & \operatorname{Re}\{\mathbf{v}\} \end{bmatrix} \begin{bmatrix} \operatorname{Re}\{\zeta\} \\ \operatorname{Im}\{\zeta\} \end{bmatrix} = 0 \Longrightarrow \mathbf{v}\zeta = 0 \Longrightarrow \mathbf{v} = 0 \tag{46}$$

which is a contradiction to the assumption that $\mathbf{v} \neq 0$.

Thus, we have shown that from each $\mathbf{v} \in \mathcal{N}(\mathbf{R})$ we can obtain (as in (44) and (45)) two linearly independent vectors in $\mathcal{N}(\tilde{\mathbf{R}})$. Furthermore, we can use an argument similar to (46) to show that if the vectors $\mathbf{v}_1, \mathbf{v}_2, \ldots \in \mathcal{N}(\mathbf{R})$ are linearly independent, then so are the corresponding vectors in $\mathcal{N}(\tilde{\mathbf{R}})$. It follows from these observations that

$$\operatorname{rank}(\mathbf{R}) = M - m \Longrightarrow \operatorname{rank}(\tilde{\mathbf{R}}) \leq 2(M-m), \quad m \in [0, M]. \tag{47}$$

Conversely, for each $\boldsymbol{\nu} \neq 0$ satisfying $\tilde{\mathbf{R}}\boldsymbol{\nu} = 0$ (i.e., $\boldsymbol{\nu} \in \mathcal{N}(\tilde{\mathbf{R}})$), we can write $\boldsymbol{\nu}$ as $[\operatorname{Re}\{\mathbf{v}^T\}\ \operatorname{Im}\{\mathbf{v}^T\}]^T$, and therefore we can build a $\mathbf{v}$ such that $\mathbf{v} \in \mathcal{N}(\mathbf{R})$. Furthermore, due to the structure of $\tilde{\mathbf{R}}$, it follows, as above, that also $[-\operatorname{Im}\{\mathbf{v}^T\}\ \operatorname{Re}\{\mathbf{v}^T\}]^T \in \mathcal{N}(\tilde{\mathbf{R}})$, and that $[\operatorname{Re}\{\mathbf{v}^T\}\ \operatorname{Im}\{\mathbf{v}^T\}]^T$ and $[-\operatorname{Im}\{\mathbf{v}^T\}\ \operatorname{Re}\{\mathbf{v}^T\}]^T$ are linearly independent of each other. Therefore, for any two such linearly independent vectors in $\mathcal{N}(\tilde{\mathbf{R}})$, there is one vector $\mathbf{v} \in \mathcal{N}(\mathbf{R})$. Again, similarly to what was shown above, the linear independence of the vectors in $\mathcal{N}(\tilde{\mathbf{R}})$ implies that of the corresponding vectors in $\mathcal{N}(\mathbf{R})$. Therefore, we have shown that

$$\operatorname{rank}(\tilde{\mathbf{R}}) = 2(M-m) \Longrightarrow \operatorname{rank}(\mathbf{R}) \leq M - m, \quad m \in [0, M]. \tag{48}$$

The stated result in (42) follows from (47) and (48). Indeed, if $\operatorname{rank}(\mathbf{R}) = M-m$, then we must have $\operatorname{rank}(\tilde{\mathbf{R}}) = 2(M-m)$ (otherwise (47) and (48) would imply that $\operatorname{rank}(\tilde{\mathbf{R}}) < 2(M-m)$, by (47), and thus that $\operatorname{rank}(\mathbf{R}) < M-m$, by (48), which is a contradiction). Similarly, (47) and (48) can be used to conclude that $\operatorname{rank}(\tilde{\mathbf{R}}) = 2(M-m) \Longrightarrow \operatorname{rank}(\mathbf{R}) = M-m$. □

The above lemma is related to a number of results in [17] for matrices of the form of (35), but it does not appear in the cited paper. In fact, while the lemma's result may possibly be known, we have not been able to locate it in the literature, and this is why we provided a proof of it in this Appendix.

Acknowledgment

The authors would like to thank the reviewers for their thoughtful and to-the-point comments and suggestions.

References

[1] E. Fishler, A. Haimovich, R. Blum, D. Chizhik, L. Cimini, and R. Valenzuela, "MIMO radar: An idea whose time has come," in *Proc. IEEE Radar Conf.*, Apr. 2004, pp. 71–78.

[2] E. Fishler, A. Haimovich, R. Blum, L. Cimini, D. Chizhik, and R. Valenzuela, "Performance of MIMO radar systems: Advantages of angular diversity," in *Proc. 38th Asilomar Conf. Signals, Syst. Comput.*, Nov. 2004, vol. 1, pp. 305–309.

[3] D. R. Fuhrmann and G. S. Antonio, "Transmit beamforming for MIMO radar systems using partial signal correlation," in *Proc. 38th Asilomar Conf. Signals, Syst. Comput.*, Nov. 2004, vol. 1, pp. 295–299.

[4] F. Robey, S. Coutts, D. Weikle, J. McHarg, and K. Cuomo, "MIMO radar theory and experimental results," in *Proc. 38th Asilomar Conf. Signals, Syst. Comput.*, Nov. 2004, vol. 1, pp. 300–304.

[5] K. Forsythe and D. Bliss, "Waveform correlation and optimization issues for MIMO radar," in *Proc. 39th Asilomar Conf. Signals, Syst. Comput.*, Nov. 2005, pp. 1306–1310.

[6] L. Xu, J. Li, and P. Stoica, "Radar imaging via adaptive MIMO techniques," presented at the EUSIPCO, Florence, Italy, 2006 [Online]. Available: fttp://www.sal.ufl.edu/xuluzhou/EUSIPCO2006.pdf

[7] E. Fishler, A. Haimovich, R. Blum, L. Cimini, D. Chizhik, and R. Valenzuela, "Spatial diversity in radars—Models and detection performance," *IEEE Trans. Signal Process.*, vol. 54, no. 3, pp. 823–838, Mar. 2006.

[8] D. R. Fuhrmann and G. S. Antonio, "Transmit beamforming for MIMO radar systems using signal cross-correlation," *IEEE Trans. Aerosp. Electron. Syst.*, submitted for publication.

[9] P. Stoica and R. Moses, *Spectral Analysis of Signals*. Upper Saddle River, NJ: Prentice-Hall, 2005.

[10] P. Stoica and G. Ganesan, "Maximum-SNR spatial-temporal formatting designs for MIMO channels," *IEEE Trans. Signal Process.*, vol. 50, no. 12, pp. 3036–3042, Dec. 2002.

[11] J. Sturm, "Using sedumi 1.02, a matlab toolbox for optimization over symmetric cones," *Optimiz. Meth. Softw.*, vol. 11–12, pp. 625–653, 1999.
[12] S. Boyd and L. Vandenberghe, *Convex Optimization*. Cambridge, UK: Cambridge Univ. Press, 2004.
[13] S. P. Wu, S. Boyd, and L. Vandenberghe, *FIR Filter Design Via Semidefinite Programming and Spectral Factorization*. Boston, MA: Birkhauser, 1998, ch. 5, pp. 215–245.
[14] T. N. Davidson, Z.-Q. Luo, and J. F. Sturm, "Linear matrix inequality formulation of spectral mask constraints with applications to FIR filter design," *IEEE Trans. Signal Process.*, vol. 50, no. 11, pp. 2702–2715, Nov. 2002.
[15] R. Orsi, U. Helmke, and J. B. Moore, "A Newton-like method for solving rank constrained linear matrix inequalities," in *Proc. 43rd IEEE Conf. Decision Contr.*, 2004, pp. 3138–3144.
[16] L. Xu, P. Stoica, and J. Li, "A diagonal growth curve model and some signal processing applications," *IEEE Trans. Signal Process.*, vol. 54, no. 9, pp. 3363–3371, Sep. 2006.
[17] N. R. Goodman, "Statistical analysis based on a certain multivariate complex Gaussian distribution (an introduction)," *Annals Math. Stat.*, vol. 34, pp. 152–177, 1963.

Petre Stoica (F'94) received the D.Sc. degree in automatic control from the Polytechnic Institute of Bucharest (BPI), Bucharest, Romania, in 1979 and an honorary doctorate degree in science from Uppsala University (UU), Uppsala, Sweden, in 1993.

He is a Professor of systems modeling with the Division of Systems and Control, the Department of Information Technology at UU. Previously, he was a Professor of system identification and signal processing with the Faculty of Automatic Control and Computers at BPI. He held longer visiting positions with Eindhoven University of Technology, Eindhoven, The Netherlands; Chalmers University of Technology, Gothenburg, Sweden (where he held a Jubilee Visiting Professorship); UU; The University of Florida, Gainesville, FL; and Stanford University, Stanford, CA. His main scientific interests are in the areas of system identification, time series analysis and prediction, statistical signal and array processing, spectral analysis, wireless communications, and radar signal processing. He has published nine books, ten book chapters, and some 500 papers in archival journals and conference records. The most recent book he coauthored, with R. Moses, is *Spectral Analysis of Signals* (Prentice-Hall, 2005).

Dr. Stoica is on the Editorial Boards of six journals: *Journal of Forecasting; Signal Processing; Circuits, Signals, and Signal Processing; Digital Signal Processing CA Review Journal*; *Signal Processing Magazine*; and *Multidimensional Systems and Signal Processing*. He was a Co-Guest Editor for several special issues on system identification, signal processing, spectral analysis, and radar for some of the aforementioned journals, as well as for *IEE Proceedings*. He was corecipient of the IEEE ASSP Senior Award for a paper on statistical aspects of array signal processing. He was also recipient of the Technical Achievement Award of the IEEE Signal Processing Society. In 1998, he was the recipient of a Senior Individual Grant Award of the Swedish Foundation for Strategic Research. He was also co-recipient of the 1998 EURASIP Best Paper Award for Signal Processing for a work on parameter estimation of exponential signals with time-varying amplitude, a 1999 IEEE Signal Processing Society Best Paper Award for a paper on parameter and rank estimation of reduced-rank regression, a 2000 IEEE Third Millennium Medal, and the 2000 W. R. G. Baker Prize Paper Award for a paper on maximum likelihood methods for radar. He was a member of the international program committees of many topical conferences. From 1981 to 1986, he was a Director of the International Time-Series Analysis and Forecasting Society, and he was also a member of the IFAC Technical Committee on Modeling, Identification, and Signal Processing. He is also a member of the Royal Swedish Academy of Engineering Sciences, an honorary member of the Romanian Academy, and a fellow of the Royal Statistical Society.

Jian Li (F'05) received the M.Sc. and Ph.D. degrees in electrical engineering from The Ohio State University, Columbus, in 1987 and 1991, respectively.

From July 1991 to June 1993, she was an Assistant Professor with the Department of Electrical Engineering, University of Kentucky, Lexington. Since August 1993, she has been with the Department of Electrical and Computer Engineering, University of Florida, Gainesville, where she is currently a Professor. Her current research interests include spectral estimation, statistical and array signal processing, and their applications.

Dr. Li is a Fellow of IEE. She received the 1994 National Science Foundation Young Investigator Award and the 1996 Office of Naval Research Young Investigator Award. She has been a member of the Editorial Board of Signal Processing, a publication of the European Association for Signal Processing (EURASIP), since 2005. She is presently a member of two of the IEEE Signal Processing Society technical committees: the Signal Processing Theory and Methods (SPTM) Technical Committee and the Sensor Array and Multichannel (SAM) Technical Committee.

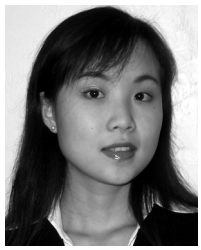

Yao Xie (S'04) received the B.Sc. degree from the University of Science and Technology of China (USTC), Hefei, China, in 2004, and the M.Sc. degree from the University of Florida, Gainesville, in 2006, both in electrical engineering. She is currently pursuing the Ph.D. degree with the Department of Electrical Engineering at Stanford University, Stanford, CA.

Her research interests include signal processing, medical imaging, and optimization.

Ms. Xie was the First Place Winner in the Student Best Paper Contest at the 2005 Annual Asilomar Conference on Signals, Systems, and Computers, for her work on breast cancer detection. She is a member of Tau Beta Pi and Etta Kappa Nu.